ADVANCED MATERIALS

Supporting Information

for *Adv. Mater.*, DOI: 10.1002/adma.202000006

2D Electrets of Ultrathin MoO_2 with Apparent Piezoelectricity

Amey Apte, Kosar Mozaffari, Farnaz Safi Samghabadi, Jordan A. Hachtel, Long Chang, Sandhya Susarla, Juan Carlos Idrobo, David C. Moore, Nicholas R. Glavin, Dmitri Litvinov, Pradeep Sharma, Anand B. Puthirath,* and Pulickel M. Ajayan**

2D Electrets of Ultrathin MoO_2 with Apparent Piezoelectricity

Amey Apte [1,8], Kosar Mozaffari [2], Farnaz Safi Samghabadi [3], Jordan A. Hachtel [4], Long Chang [5], Sandhya Susarla [1,9], Juan Carlos Idrobo [4], David C. Moore[6], Nicholas R. Glavin[6], Dmitri Litvinov [3,5], Pradeep Sharma [2,7,*], Anand B. Puthirath [1,*], and Pulickel M. Ajayan [1,*]

Affiliations

1. Department of Materials Science & NanoEngineering, Rice University, 6100 Main Street, Houston, TX – 77005, United States.
2. Department of Mechanical Engineering, University of Houston, 4726 Calhoun Road, Houston, TX – 77204, United States.
3. Materials Science and Engineering Program, University of Houston, 4726 Calhoun Rd, Houston, TX – 77204, United States.
4. Center for Nanophase Materials Science, Oak Ridge National Laboratory, Oak Ridge, TN – 37831, United States.
5. Department of Electrical and Computer Engineering, University of Houston, Houston TX – 77204, United States.
6. Materials and Manufacturing Directorate, Air Force Research Laboratory, Wright-Patterson AFB, OH, 45433 USA
7. Department of Physics, University of Houston, 3507 Cullen Blvd, Houston, TX – 77204, United States.
8. Intel Corporation, 5000 W Chandler Blvd, Chandler, AZ-85226
9. Materials Sciences Division, Lawrence Berkeley National Laboratory, 1 Cyclotron Rd, Berkeley, CA 94720

Email for correspondence: ajayan@rice.edu, psharma@central.uh.edu, anandputhirath@rice.edu

Nano-indentation experiments

In order to model and interpret the piezo-response of the ultra-thin MoO_2 flakes, we estimated mechanical properties such as modulus ($E_{r)}$ and hardness (H) via nanoindentation measurements using a Hysitron TI 980 Tribo-Indenter with a 150 nm Berkovich probe. A: To nullify the substrate effect, the penetration of indenter probe was limited to <1/4th of the thickness of the sample. To facilitate this protocol, we have performed the indentation on slightly thicker samples (10-20 nm)

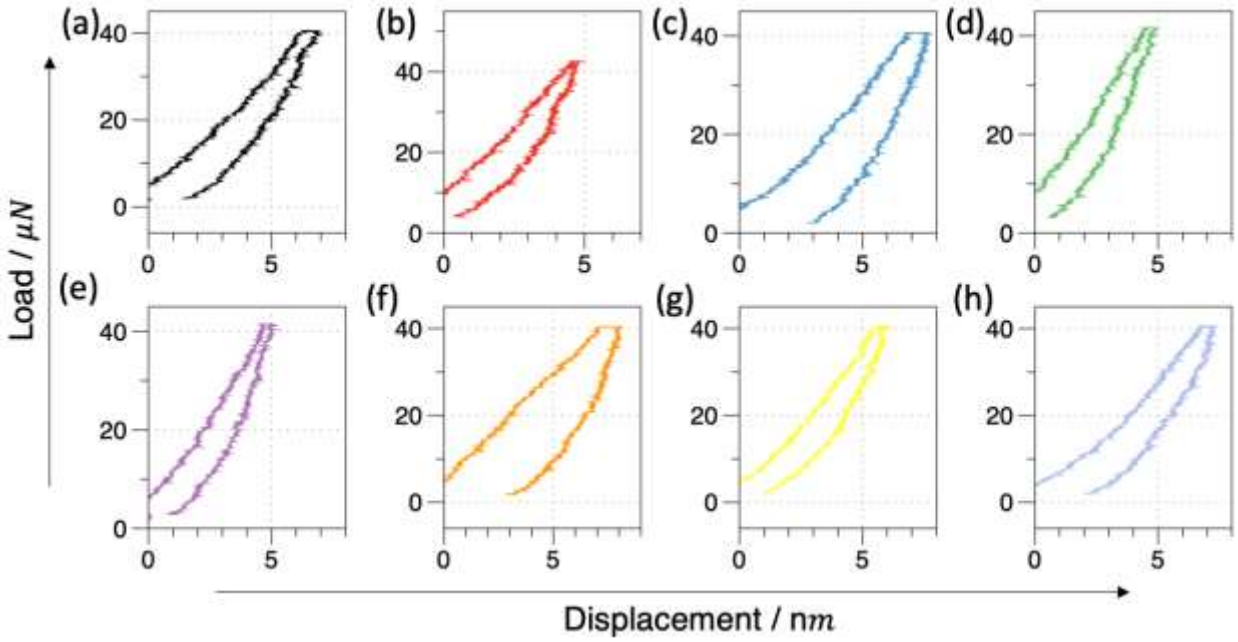

SI Figure 1 (a-h) Load-displacement curves of eight nano-indentation experiments on different MoO_2 flakes.

The single indents were made via a built-in basic QS trapezoid load function with a maximum load 40 μN. The results of the nanoindentation measurements are displayed in **SI Figure 1** whereas the AFM images of an example flake with the indent shape are shown in **SI Figure 2**. The reduced modulus (E_R*) and Hardness (H) were measured to be 103.25 ±8.26 GPa and 2.13 ± 0.11 GPa respectively.

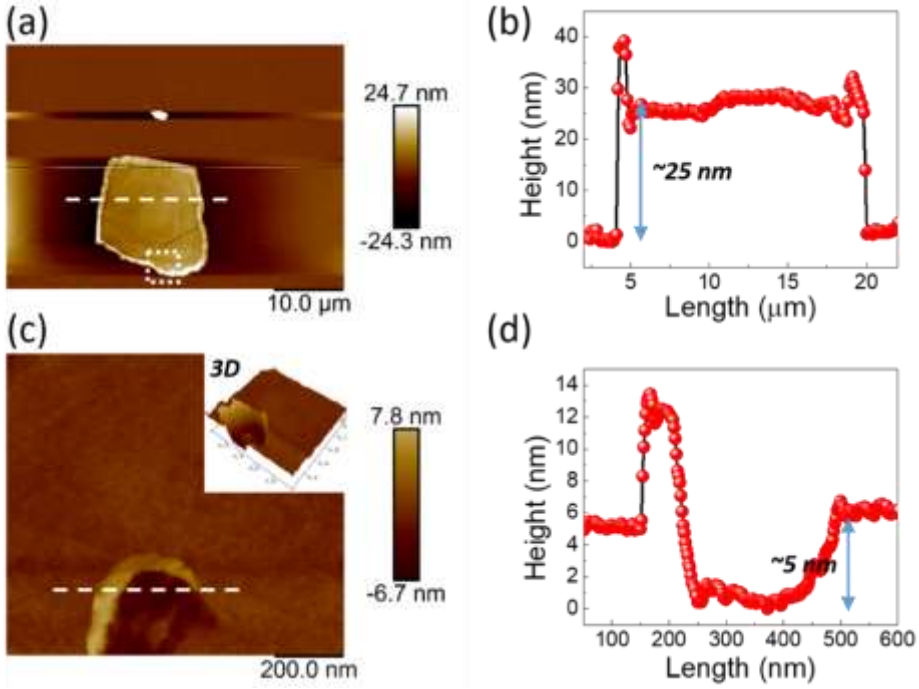

SI Figure 2 AFM images of nano-indented flakes showing corresponding depth of single indent.

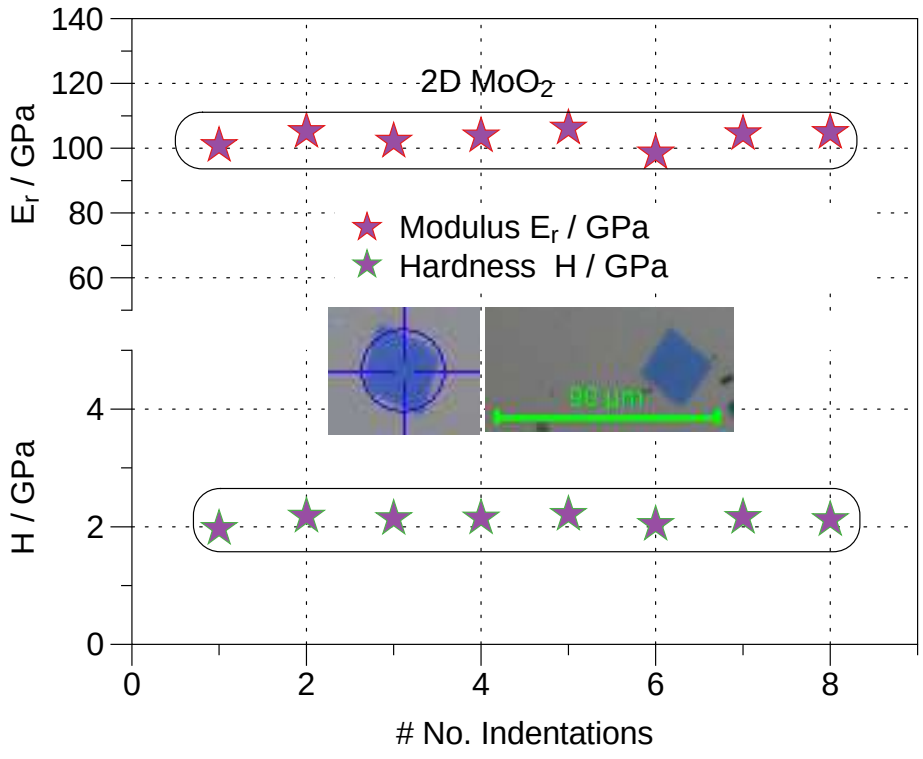

SI Figure 3 The Modulus and hardness values obtained for several MoO_2 flakes are graphed and compared. Inset: Optical microscope images of MoO_2 flake and a flake on Si/SiO_2 substrate.

Thus, the indentation protocol followed and the observations thereby nullify the chance of contribution of the substrate towards the measured mechanical properties of the MoO_2 samples.

Theoretical modeling details

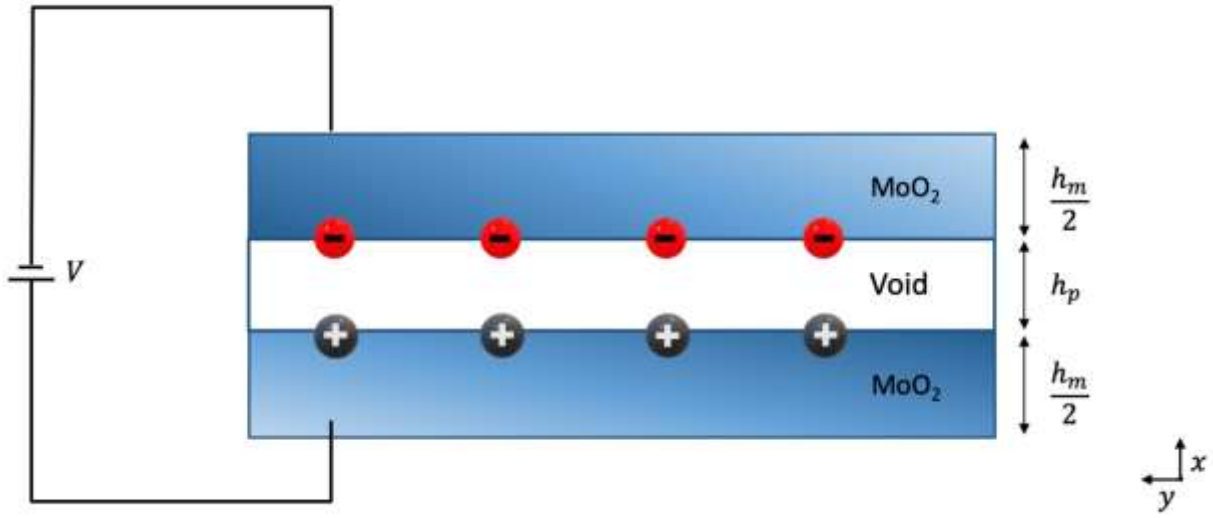

SI Figure 4 Schematic of MoO_2 layers with layer of air in between, subject to the voltage difference V. Opposite charges are deposited in the interface of the void with MoO_2 layers.

In this part, we are mainly following the discussion by Deng et al with some modifications. [1] We can mimic the central physics of the system by a triple layer arrangement as shown in ***SI Figure 4*** The upper and lower layers are made of MoO_2 material and the middle layer is a void representing the defect. The charges (q_0) are deposited on the upper and lower interface of the middle layer. If this system undergoes a deformation, since the stiffness of the hard material is much larger than stiffness of the void, the deformation is expected to mostly take place in the void layer. This rational assumption concludes that the MoO_2 layers carry negligible part of the deformation and the strain will be close to zero in related layers.

We assume that the voltage difference across the each MoO_2 (void) layer is shown with V_m (V_a). Therefore, the voltage difference across the whole material will be $V = V_a + 2V_m$. From Maxwell's equation we have:

$$-\epsilon_0 \frac{V_a}{h_a} + \epsilon_m \frac{V_m}{h_m} = -q_0$$

Eliminating V_m from this equation will result in:

$$\frac{V_a}{h_a} = \frac{q_0 h_m + \epsilon_m V}{\epsilon_0 h_m + \epsilon_m h_a}$$

The balance of linear momentum in absence of any external surface traction or body force gives:

$$(\lambda_a - 1)E_a + t_1^{MS} = 0$$

$$(\lambda_m - 1)E_m + t_2^{MS} = 0$$

Where λ_a , λ_m and t_i^{MS} are the average stretches and Maxwell stresses associated with each layer are as follows:

$$\lambda_a = 1 + \frac{u_a}{\mathrm{H}_a}\ , \qquad \lambda_m = 1 + \frac{u_m}{\mathrm{H}_m}$$
$$t_1^{MS} = \frac{1}{2}\epsilon_0 \left(\frac{V_a}{h_a}\right)^2, \qquad t_2^{MS} = \frac{1}{2}\epsilon_m \left(\frac{2V_m}{h_m}\right)^2$$

Using the result of balance of linear momentum for the void layer and substituting Maxwell stress, we arrive at:

$$\frac{H_a}{H_a + H_m}(\lambda_a - 1)E^* + \frac{1}{2}\epsilon_0 \left(\frac{V_a}{h_a}\right)^2 = 0$$

Substituting the stretch, $\frac{V_a}{h_a} = \frac{q_0 h_m + \epsilon_m V}{\epsilon_0 h_m + \epsilon_m h_a}$ and $v_f = \frac{H_a}{H_a + H_m}$ then solving it for the deformation we find that:

$$u = -\frac{\epsilon_0 H_a}{2 v_f E^*}\left(\frac{q_0 h_m + \epsilon_m V}{\epsilon_0 h_m + \epsilon_m h_a}\right)^2$$

The effective piezoelectric coefficient can be obtained by measuring the change of thickness with respect to the change in the applied voltage evaluated at zero voltage, i.e. $d_{eff} = \left.\frac{du}{dV}\right|_{v\to 0}$. Therefore, the apparent piezoelectric coefficient can then be calculated to be:

$$d_{eff} = \frac{-\epsilon_0 \epsilon_m H_a}{v_f E^*} \left.\frac{q_0 h_m + \epsilon_m V}{(\epsilon_0 h_m + \epsilon_m h_a)^2}\right|_{v\to 0} = \frac{-\epsilon_0 \epsilon_m H_a H_m q_0}{v_f E^* (\epsilon_0 H_m + \epsilon_m H_a)^2}$$

Additional STEM Analysis

To verify that the flakes are indeed the structure as determined by XRD, we compare the atomic-resolution high-angle annular dark field STEM images with a monoclinic $P2_{1/c}$ (Tugarinovite) structure. The [201] projection of the Tugarinovite phase is shown in **SI Figure *5*** (a), and the experimental STEM image of a similar sized region is shown in **SI Figure *5*** (b). The crystal structure is a clear match, and even the O bridges between Mo doublets can be observed at most sites.

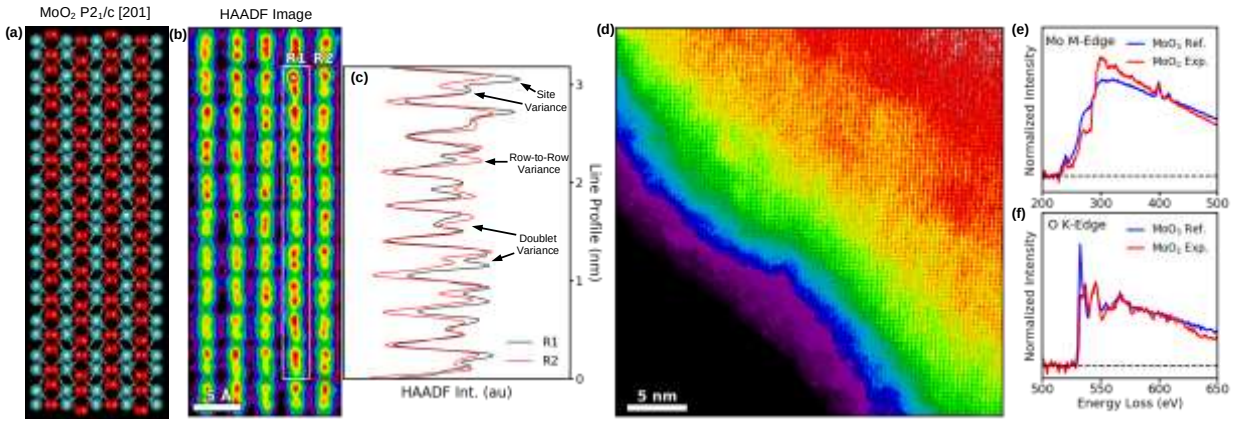

SI Figure 5 (a) Schematic [201] projection of MoO_2 in a Tugarinovite phase with monoclinic $P2_1/c$ structure. (b) Experimental HAADF STEM image showing same crystal structure. (c) Line profile of adjacent rows of Mo-doublets exhibiting extensive atomic scale contrast variation. (d) Large area image of MoO_2 flake demonstrating that varying stoichiometry is present across entire sample. (e,f) Core-loss EELS measurements from MoO_2 flake compared to MoO_3 reference data from Ahn et al [2], showing that synthesized material is MoO_2.

Additionally, line profiles of two different Mo-rows are plotted in **SI Figure 5** (c) to help clearly demonstrate the high degree of atomic-scale variation present in the HAADF intensity. Here, it can be seen that there is variation in the HAADF intensity between neighboring doublets in the same row and in adjacent rows, and frequently between the two Mo columns in each doublet.

This level of contrast can be observed across large areas of the sample as well as observed in **SI Figure 5** (d). Here, since we image a large region, the thickness gradient of the flake dominates the contrast, but by examining areas of comparable thickness (running parallel to the edge) it can be seen that significant atomic-scale contrast can be observed at all places across the entire sample.

Lastly, the MoO_2 flakes are characterized with core-loss electron energy-loss spectroscopy (EELS) and compared to reference data for the more standard MoO_3 structure taken from Ahn et al [2]. In **SI Figure 5** (e), we see the Mo M-edge 226 eV for the reference and experimental data,

while some small changes in the fine-structure of the edge are observable the edge is largely masked by the presence of the Carbon K-edge peak at 288 eV. The O K-edge shown in **SI Figure 5** (f) is clearer, and shows significant difference in the fine-structure at the K-edge onset. This onset is in good agreement with other published O K-edge fine structure EELS data [3]

Raman and XPS spectrum of MoO_2 sample post-annealing

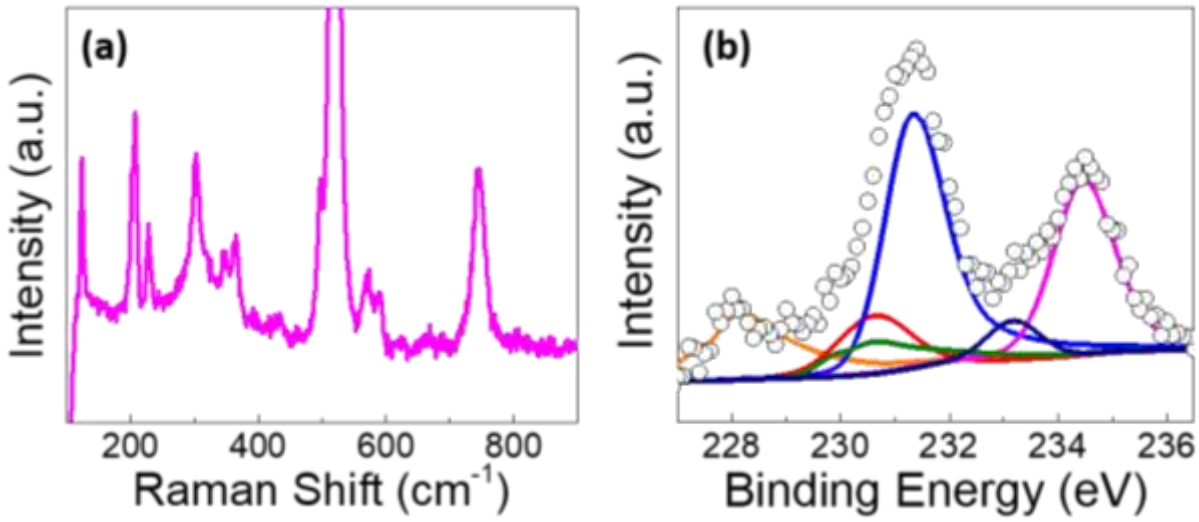

SI Figure 6 (a) Raman and (b) XPS Mo 3d spectra of the post-annealed MoO_2 sample. The peaks at 521 cm^{-1} and 301 cm^{-1} are due to underlying substrate.

The Raman and XPS spectra of the MoO_2 sample were recorded after the annealing treatment; they are shown in SI Figure 6. Compared the Raman spectrum of the sample in Figure 1 (c), there are no significant changes (i.e. appearance of new peaks, disappearance of existing ones). More specifically, there are no peaks at 822 cm^{-1} and 667 cm^{-1} which are strong for MoO_3. The XPS for the Mo 3d region shows some difference compared to Figure 1(f). Specifically, the intensities of the $3d_{5/2}$ doublets from Mo 4+ oxidation states at 228.2 eV and 230.7 eV has decreased with a relative increase in the corresponding $3d_{5/2}$ peak from Mo 6+ region at 231.3 eV. The initial assumption would be the increased presence of MoO_3 oxide, however that is not

seen significantly in the Raman spectrum as discussed. Therefore, a plausible reason would be as follows: the origin of electret-based piezo-response in CVD MoO_2 is explained due to presence of trapped charges in the defects. These are attributed to the charges on oxygen anions in the lattice. Annealing the sample provides sufficient energy to reform the oxygen-molybdenum bonds thus reducing the negative charges on the anions (or the charge densities near the defects) and thereby increasing the coordination number of the Mo atoms. This manifests in the changes that are consistent with the observations in Raman and XPS spectra and stand as the reason for the homogenization of converse piezo response.

Temperature dependence of electrical conductivity

Lithography and Au deposition were used to fabricate contacts to individual MoO_2 flake on SiO_2/Si substrates. The room temperature I-V curve of MoO_2 flake with zero gate voltage is shown in Fig.6(c) . The linear/ ohmic variation is indicative of metallic conduction. The slope of the curve gives an ultra-low resistance value as 175Ω. I-V curves were measured during warming at regular temperature intervals between 90-400K and the slopes were used to calculate the resistance values. A plot of the resistance as a function of temperature is shown in Fig. 6(d). As expected for a metallic conductor, the resistance decreases with decreasing temperature. Moreover, there is a cusp in the curve at T = 280K which corresponds to the observation of a non-structural transition as reported by Alves et al for bulk single-crystals.[4] The overall curve was fit to the following Bloch-Gruneisen relation:

$$R(T) = R(0) + A\left(T/\theta_R\right)^n$$

Here, $R(0)$ is the resistance at $T = 0K$, θ_R is the Debye temperature, and n is the exponent. We obtain a goodness of fit (R^2) = 0.97. We obtain of θ_R = 7.6K and exponent value of 2.31 which is typical of transition metal-like conductivity.

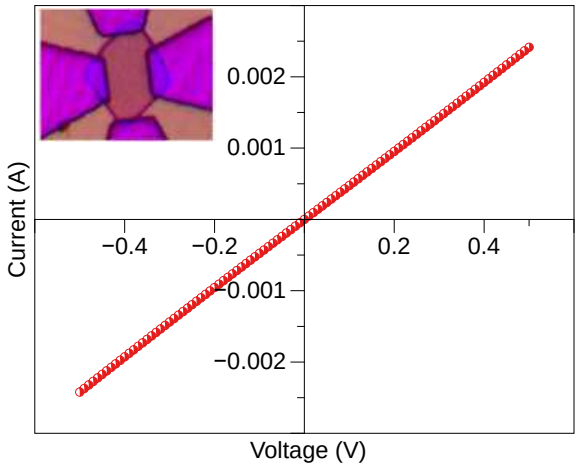

SI Figure 6 (c) I-V characteristics of MoO_2 at room temperature showing metallic conductivity. The inset shows optical image of a single flake and the patterned contacts before metal deposition.

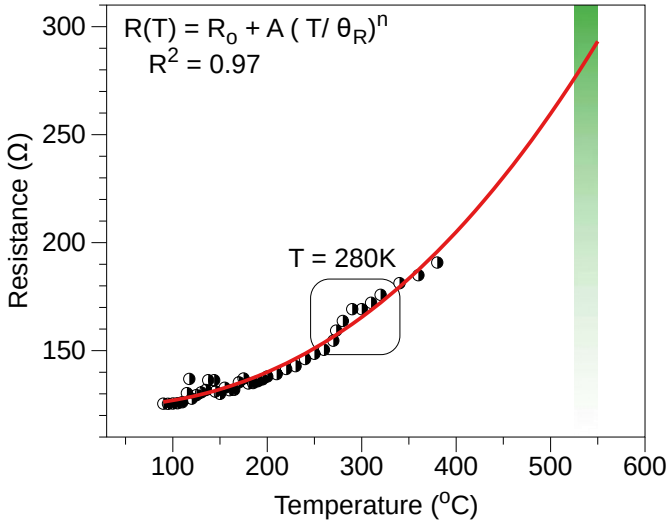

SI Figure 6 (d) Temperature-dependent resistance of MoO_2 flake showing metallic behavior fitted to Bloch-Gruneisen relation.

Thus, at 550K, the expected resistance value will be 293.18 Ω. This shows that the variation of electrical resistance during the annealing procedure is hardly contributing towards the piezoelectric behaviour of the sample. Therefore, the homogenization of the charges is fundamentally originated due to reformation of the oxygen-molybdenum bonds which in turn

define the distribution of trapped charges and their contribution towards the converse piezoelectric behaviour.

Piezo-response Force Microscopy (PFM) : Extended Study

At different dc biases

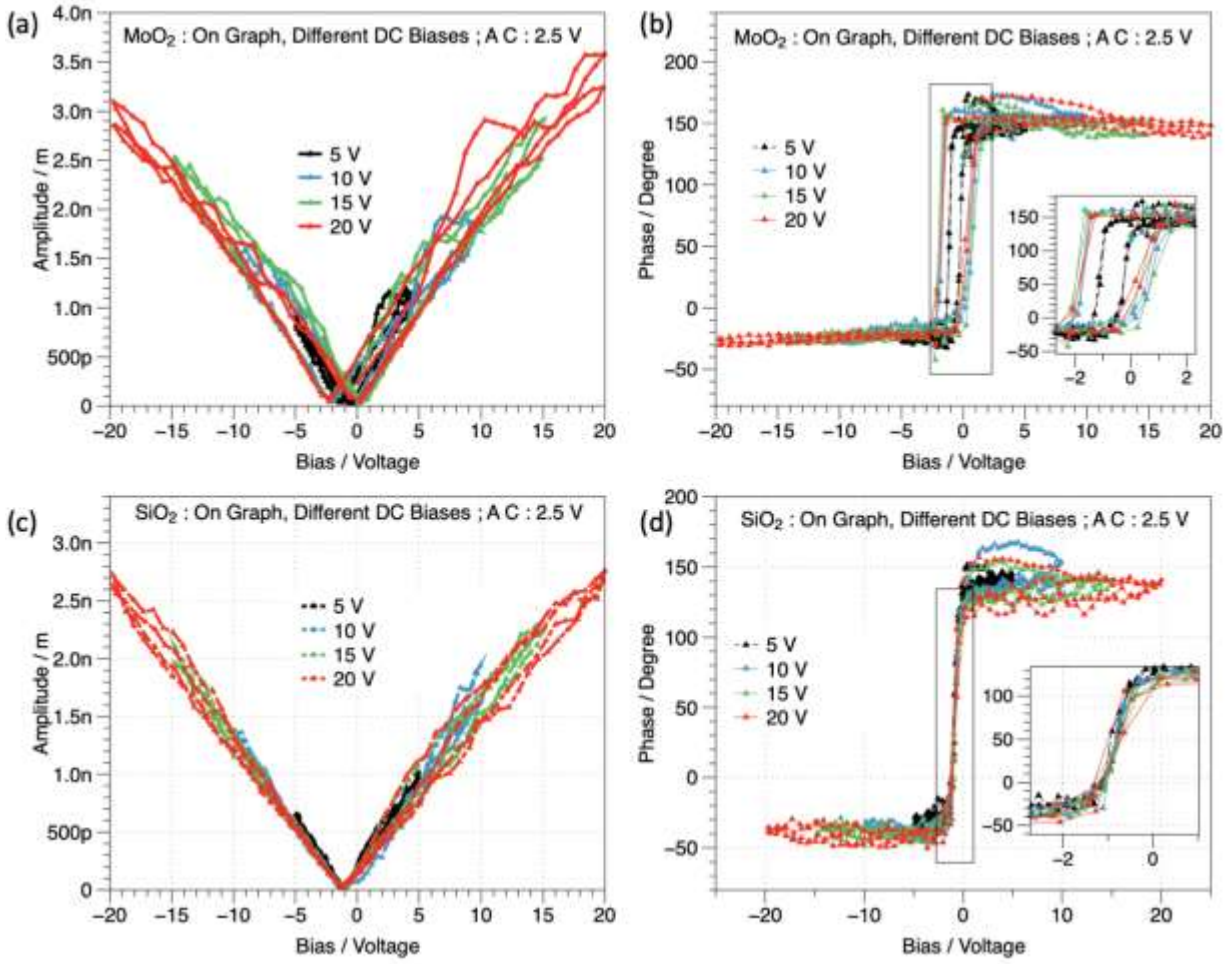

SI Figure 6 Comparison of the on-field amplitude (a and c) and phase (b and d) response of MoO2 flake and SiO2 substrate at AC deriving voltage of 2.5 V and different DC biases.

We have also made additional measurements using different dc biases that further show the differences in the PFM response of MoO_2 and SiO_2/Si substrate, see the plots depicted in **SI Figure *6***. The MoO_2 shows characteristic piezoelectric behavior such as butterfly amplitude loops and 180 degrees phase flips with hysteresis. On the other hand, SiO_2/Si substrate does not

show a butterfly loop in the amplitude plot or hysteresis in the phase plot. In addition, the amplitude response of the MoO2 is approximately 2 times larger than the SiO_2/Si substrate. Therefore, it is unlikely that the PFM data of MoO_2 is heavily influenced by the SiO_2/Si substrate.

At On-Off Fields

The measured PFM response is a combination of ferroelectric-like behavior from trapped charges and electrostatic forces between the tip and the sample.

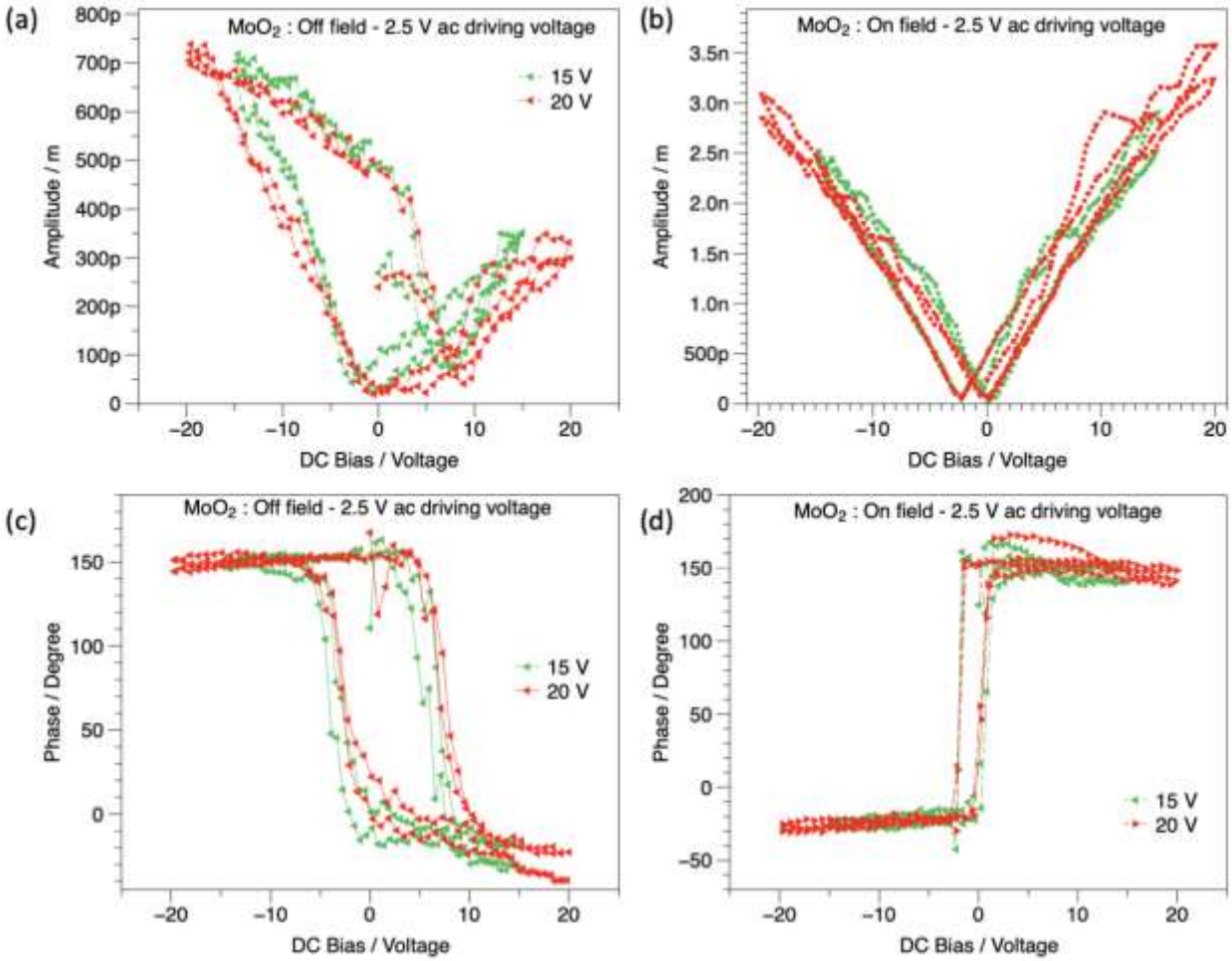

SI Figure 7 Amplitude (a) on-field, (b) off-field and phase (c) off-field, (d) on-field of MoO2 flakes under fixed AC driving voltage of 2.5 V and two different DC biases.

Charge is injected onto the sample when a DC bias is applied on the tip. These injected charges push against the cantilever producing a PFM amplitude signal. The injected charges dissipate very quickly off the semi-metallic MoO_2 surface. This is supported by the similarities of the amplitude plot at a DC bias of 15V and 20V. Below 15V, the plots for 15V and 20V are the same (**SI Figure 7**). Beyond 15V, the amplitude increases as more charge is injected. As we sweep back from 20V to 15V, the additional injected charge must dissipate for the amplitude plots to match at 15V and below. Since the DC field sweep from 20V to 15V takes 120 ms, the injected charge dissipation rate must be faster.

This is further examined in the Voltage ON vs the Voltage OFF measurement. For the Voltage ON plot, the DC bias is turned on during the PFM measurement. For the Voltage OFF plot, the DC bias is turned on and then turned off before performing PFM measurement. If the injected charge dissipation is really fast, the PFM measurements for Voltage OFF shows the ferroelectric-like response of trapped charges in MoO_2. The phase and amplitude plots are identical at different biases, so the Voltage OFF PFM measurements do not appear to be affected by injected charges. On the other hand, the Voltage ON PFM measurements show a completely different behavior with approximately 3.5 times larger amplitude at 15V DC and a significantly narrower hysteresis loop. One argument that can explain the narrower hysteresis loop is that charges injected to the surface during on-field measurement may generate an electric field which forces a greater number of dipoles to polarize simultaneously and consequently reduces the polarization switching field. Removing that field limits the electric field to one single point beneath the cantilever tip and fewer dipoles. Therefore, a higher voltage is needed for all the dipoles to align with the field.

Variation of Piezo amplitude with applied AC voltages

Another method that further confirms the piezoelectric nature of the PFM response is the linear change of the amplitude with AC driving voltage derived from scanning a single flake, when no dc bias is applied to it.

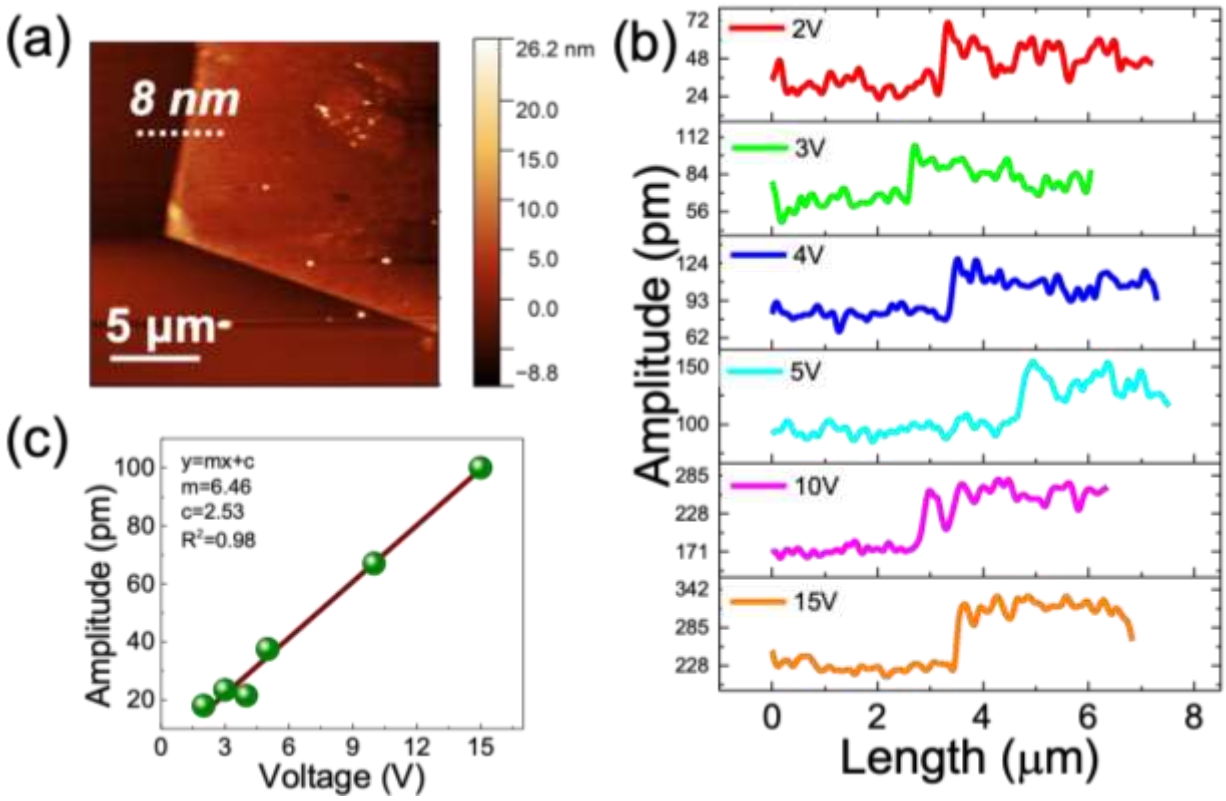

SI Figure 8 Piezo-amplitude changes in an (a) 8 nm thick MoO_2 flake with (b) different driving voltages from 2V to 15V. (c) linear relationship between the amplitude and driving voltage.

The figure above shows the relationship between measured piezo-amplitude and driving voltage. **SI Figure *8*** (a) shows the topography of a single crystalline MoO_2 flake with thickness of ~ 8 nm. This flake was scanned at different driving voltages to measure the piezo-amplitude. **Error! Reference source not found.** (b) shows line scans of the amplitude (measured in picometers) as a function of the voltage (different colors) ranging from 2V to 15V. We observed that the amplitude increased proportionately with the voltage, with the increasing step height clearly

visible and measurable in the plot. **SI Figure *8*** (c) shows the amplitudes as a function of voltages. A linear relationship can be established to a very good accuracy ($R^2 \sim 0.98$).

Kelvin Probe Force Microscopy (KPFM)

To ensure that charge was not trapped in the MoO_2, KPFM was conducted to observe charge relaxation (**SI Figure *9***). A desired potential was applied via back-gating for 15 minutes. Electrons tunneled through the thin SiO_2 layer on the substrate to accumulate until interface reached equilibrium. KPFM measures the contact potential difference between a nanoscopic probe and the sample, which is due to the work function plus accumulated charge. Uncharged MoO_2 was measured at around 200 mV relative to the silicon probe, thus almost all of the observed surface potential was due to charging. No attempt was made to quantify this charge as an unknown amount of MoO_2 was on the surface.

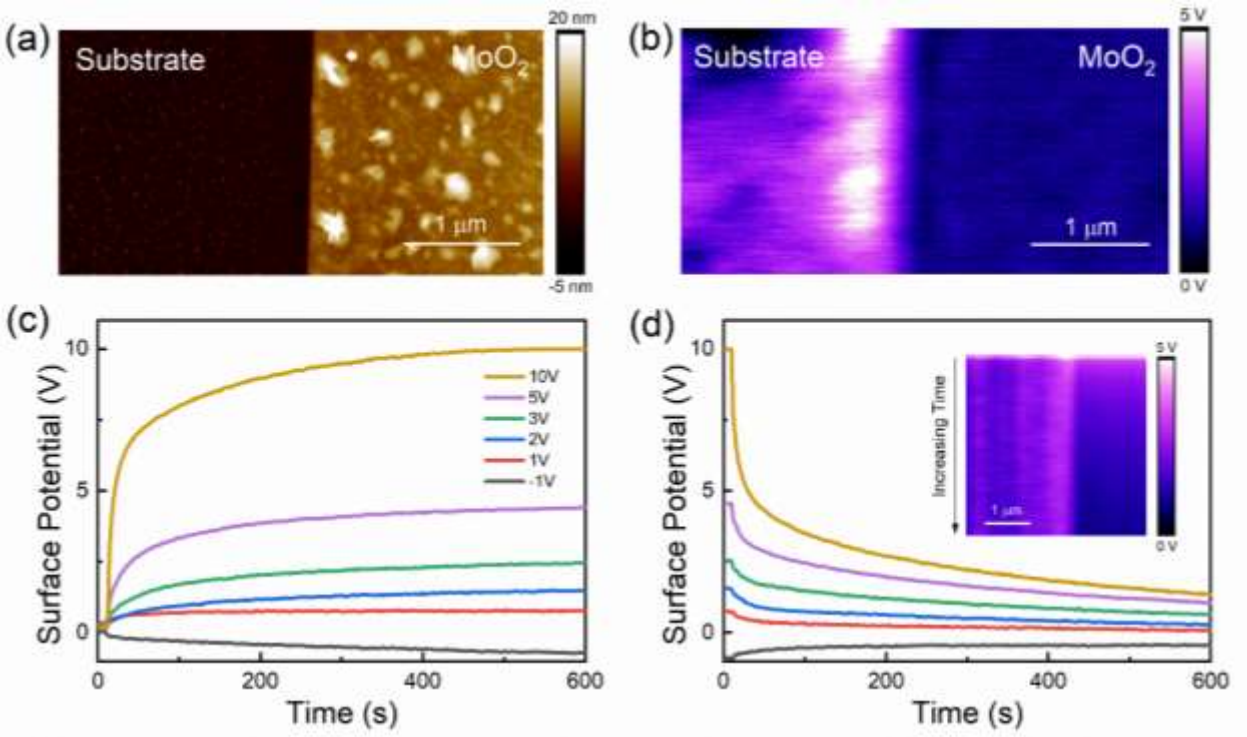

SI Figure 9 KPFM of a MoO_2 flake edge with simultaneous (a) topography and (b) surface potential. (c) Surface potential increasing with charging and (d) decreasing with discharging over time. (d inset) A KPFM scan repeated over a single line to create horizontal position vs time.

The probe was scanned over a single line at 977 mHz, for 11.5 minutes. The MoO_2 region's surface potential was averaged for each line. Both in charging and discharging, the initial response was fairly rapid, with >50% of the charge dissipating in the first minute. The derived decay rate is around ~4-5 V/s (slope of the decay curve just after the turn off event) and this demonstrates that charge accumulation in the MoO_2 is transitory. Similar results were qualitatively observed in a different MoO_2 flakes.

Full KPFM scans of the flake were conducted both under charge and without (**SI Figure *10***). After the flake is charged and discharged, a trapped charge was evident as a "halo" in the SiO_2 surrounding the MoO_2 flake (**SI Figure *10 (c)***). This accounts for the slowness in the relaxation after the initial drop as the surrounding SiO_2 became a charge source for the flake. Further away

from the MoO_2, the SiO_2 remains approximately 1V regardless of applied potential. Surface features such as the surface multilayers are present, but washed out due to the high potential contrast of the MoO_2 to SiO_2. **SI Figure *10*** was recorded after the time relaxation tests, so the surrounding SiO_2 already had accumulated charge,

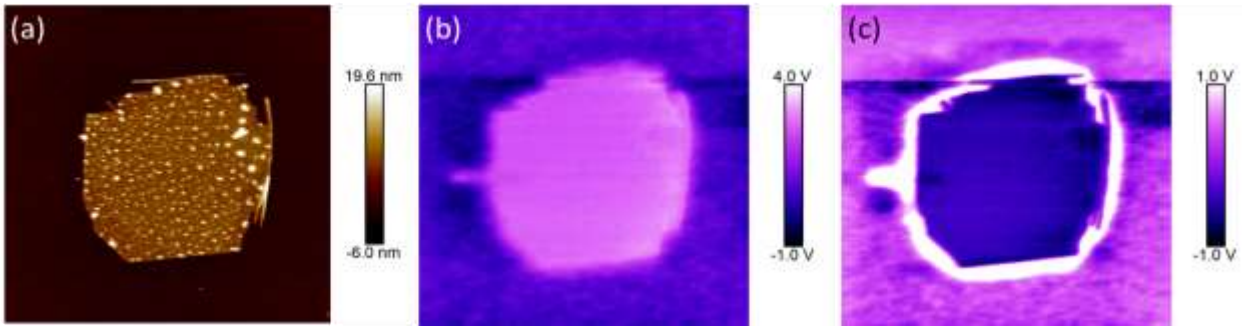

SI Figure 10 KPFM of a MoO_2 flake under (b) 5V applied potential and (c) 0V applied potential after charging. The distinct line in (c) is due to the probe contacting the surface and causing a temporary charge. The scan direction is down.

Though the trapped charges are observed at SiO_2 surrounding the MoO_2 flake, no difference in piezo amplitude is observed while scanning from the bulk to the edge of the flake. On reading these observations together , one can conclude that, charge injection /trapping is hardly contributing towards the piezo amplitude.

References

1. Deng, Q., Liu, L. & Sharma, P. Electrets in soft materials: Nonlinearity, size effects, and giant electromechanical coupling. *Phys. Rev. E* **90**, 12603 (2014).
2. Ahn, C. C. *et al. EELS atlas : a reference collection of electron energy loss spectra covering all stable elements*. (HREM Facility, Center for Solid State Science, Arizona State University ; Gatan, Inc., 1983).

3. Wang, D., Su, D. S. & Schlögl, R. Electron Beam Induced Transformation of MoO3 to MoO2 and a New Phase MoO. *Zeitschrift für Anorg. und Allg. Chemie* **630**, 1007–1014 (2004).

4. Alves, L. M. S.; Oliveira, F. S.; de Lima, B. S.; da Luz, M. S.; Rebello, A.; Masunaga, S. H.; Neumeier, J. J.; Giles, C.; Leão, J. B.; dos Santos, C. A. M. *J. Alloys Compd.* **2017**, *705*, 764–768.